

ARTICLE TEMPLATE

Optimal Control of Reserve Asset Portfolios for Pegged Digital Currencies

Alexander Hammerl^a and Georg Beyschlag^b

^aTechnical University of Denmark, Department of Management Engineering, Bygningstorvet 358, Kgs. Lyngby, 2800, Denmark; ^bTechnical University of Munich, Arcisstraße 21, Munich, Germany

ARTICLE HISTORY

Compiled August 14, 2025

ABSTRACT

Stablecoins promise par convertibility, yet issuers must balance immediate liquidity against yield on reserves to keep the peg credible. We study this treasury problem as a continuous-time control task with two instruments: reallocating reserves between cash and short-duration government bills, and setting a spread fee for either minting or burning the coin. Mint and redemption flows follow mutually exciting processes that reproduce clustered order flow; peg deviations arise when redemptions exceed liquid reserves within settlement windows. We develop a stochastic model predictive control framework that incorporates moment closure for event intensities. Using Pontryagin's Maximum Principle, we demonstrate that the optimal control exhibits a bang-off-bang structure: each asset type is purchased at maximum capacity when the utility difference exceeds the corresponding difference in shadow costs. Introducing settlement windows leads to a sampled-data implementation with a simple threshold (soft-thresholding) structure for rebalancing. We also establish a monotone stress-response property: as expected outflows intensify or windows lengthen, the optimal policy shifts predictably toward cash. In simulations covering various stress test scenarios, the controller preserves most bill carry in calm markets, builds cash quickly when stress emerges, and avoids unnecessary rotations under transitory signals. The proposed policy is implementation-ready and aligns naturally with operational cut-offs. Our results translate empirical flow risk into auditable treasury rules that improve peg quality without sacrificing avoidable carry.

KEYWORDS

Stablecoin; peg stability; reserve management; stochastic optimal control; model predictive control; hawkes processes; liquidity risk; cryptocurrency

1. Introduction

Stablecoins have become an indispensable component of the infrastructure of crypto-asset markets and an increasingly relevant settlement rail beyond them. Their defining promise is par convertibility to a more traditional asset, usually a fiat currency or a commodity, on demand. Fulfilling that promise requires an issuer to satisfy redemptions promptly while earning sufficient carry on reserves to operate sustainably. Regulatory agencies typically restrict issuers to a narrow range of permissible reserve assets.

For example, the recently enacted U.S. GENIUS Act [1] requires that stablecoin issuers pegged to the US dollar hold currency reserves exclusively in cash, short-term US government bonds, or overnight repurchase agreements thereof. In operational terms, this creates a treasury policy problem: how much of the reserve to hold as immediately available cash versus short-duration government bills, and how to set mint and burn spreads that help absorb order-flow imbalances without creating persistent departures of the secondary-market price from one. This paper develops a continuous-time framework that treats reserve allocation and fee setting as joint controls under stochastic mint and redemption flows. The objective is to minimize peg deviations and trading frictions while preserving yield, with policies designed to be implementable within daily treasury workflows.

While fiat-backed stablecoins operate outside the full decentralization paradigm, their treasury management problem intersects with broader dynamics in decentralized finance (DeFi). A literature review by [2] identifies stablecoins as a central class of "financial tokens" in DeFi, emphasizing that even fully collateralized designs can deviate from their peg, exhibit state-dependent volatility, and depend critically on liquidity provision and external data feeds. This positioning situates issuer reserve policies alongside on-chain mechanisms, market microstructure effects, and inter-protocol linkages that can amplify or dampen peg pressures.

Related market-design research links validator and block-builder incentives to liquidity and price stability in on-chain asset markets. [3] show that block-production timing strategies can yield measurable gains in maximal extractable value (MEV) without necessarily harming consensus stability. For pegged digital assets that rely on on-chain liquidity pools, MEV-maximizing behaviors among market participants can affect execution quality for redemptions and rebalancing, introducing another stochastic element into to the issuer's reserve-management problem.

[4] show that well-connected crypto funds can boost token valuation and long-run performance, suggesting that similar strategic engagement with liquidity providers and market-makers could strengthen stablecoin reserve-management.

Recent empirical work clarifies why issuers must carefully manage both their mint-and-burn policies and reserve assets, even for fully collateralized digital currencies. [5] documents that while the mean cryptocurrency issued in an initial coin offering (ICO) can deliver positive long-run buy-and-hold returns, the median token loses roughly 30% of its value over one to twenty-four months, with large issuances more often overpriced and underperforming. [6] use high-frequency data to show that no major stablecoin is absolutely stable, that return variance is non-zero, and that volatility is state dependent. Related studies document that stability varies meaningfully across designs and over time [7, 8], and that some stablecoins can act as conditional diversifiers or safe havens relative to Bitcoin during stress [9, 10]. These findings imply that operational choices inside the issuer, such as cash buffers, rebalancing cadence, and fee schedules, can shape realized peg behavior observed in secondary markets.

Price formation around the peg can be modeled by combining primary arbitrage with secondary-market order-flow dynamics. [11] formalizes a fully collateralized environment in which arbitrage against the issuer and trend-following demand interact with deviations from fundamental value. Empirically, peg deviations and trend variables predict short-horizon returns when extreme observations are retained, while explanatory power shrinks once large dislocations are trimmed [11]. This pattern is consistent with frictions and regime-like behavior, and it motivates state-dependent fee and inventory policies that anticipate clustered dislocations rather than treating all deviations as transitory noise.

A second body of evidence connects visible stablecoin flows to activity in major crypto assets. [12] study 1,587 on-chain stablecoin transfers of at least one million U.S. dollars and find significant abnormal increases in Bitcoin trading volume around these transfers. High-frequency work on Tether corroborates flow-through to returns and microstructure [13], and pandemic-period analyses report regime-dependent behavior consistent with liquidity demand and risk rebalancing [14]. These results support modeling mint and redemption dynamics as first-order drivers of liquidity demand that issuers must be prepared to meet.

The causal direction between issuance and prices remains debated. [15] present evidence that Tether flows arrive after downturns and predict positive subsequent Bitcoin returns; [16] also report issuance-related effects on Bitcoin. In contrast, [17] finds that issuance largely reacts to crypto price moves, with weak net spillovers from stablecoins to major crypto assets once contemporaneous correlations are controlled. Both mechanisms can surface in different market states, which is consistent with a policy problem in which the issuer prepares for rare but severe clustering of outflows without sacrificing unnecessary carry in normal conditions.

Macro-financial conditions further shape stablecoin behavior and the reserve allocation trade-off. [18] document that increases in interbank rates compress prices and volatility of leading stablecoins while raising both price levels and volatility of traditional cryptocurrencies; trading activity increases across both groups. Beyond market microstructure, general-equilibrium perspectives suggest that widespread adoption can carry macroeconomic implications for money and credit [19]. For fiat-backed issuers, rate regimes move the opportunity cost of holding cash relative to short-duration government bills. When redemption risk is elevated, the opportunity cost of liquidity is not static; it shifts with the interest-rate environment in ways that directly influence the optimal cash share.

Connectedness across stablecoins introduces sector-level channels of stress transmission and substitution. [20] propose complementary stability metrics and show that large USD-backed coins transmit stability conditions to smaller peers. Studies of safe-haven and hedging properties also reveal state dependence across assets and sectors [10], with COVID-era work on gold-backed tokens highlighting additional substitution and spillover channels [21–23]. These insights justify scenario designs in which a few dominant issuers shape the overall flow environment faced by the sector.

Stress episodes in non-fiat-backed designs provide quantitative benchmarks for operational frictions, capacity constraints, and governance responses. [24] analyze Maker-DAO around March 2020 and document how congestion concentrated liquidations into narrow windows and reduced auction effectiveness. The Terra–Luna collapse illustrates a distinct failure mode. [25] develops a continuous-time account linking burn dynamics and suspension beliefs; [26] assemble a high-frequency timeline of the unwind; and recent modeling of algorithmic stablecoin volatility complements these post-mortems [27]. While our scope is fiat-backed issuers operating with high-quality reserves, these episodes underscore the need for explicit, stress-aware liquidity policy at intra-day horizons and motivate the inclusion of settlement windows, queueing effects, and friction costs in our objective.

The remainder of the paper is structured as follows. Section 2 (Reserve Management Framework) introduces the reserve-eligibility set, the regulatory liquidity hierarchy, the dynamic reserve model with peg dynamics, and the state and control variables used throughout. Within Section 2, Subsection 2.2 develops the dynamic reserve model that links flows, liquidity, and peg deviations. Section 3 develops the solution approach, including stochastic model predictive control, the Pontryagin conditions that generate

feedback policies, and a settlement-window implementation; the sampled-data control used in practice is detailed in Subsection 3.3. Section 4 specifies scenarios and parameters, compares the controller with liquidity- and yield-focused benchmarks, and reports sensitivity analyses. Section 5 concludes.

2. Reserve Management Framework

2.1. Regulatory Requirements

Regulatory authorities worldwide enforce stringent requirements concerning the asset classes permissible as collateral for stablecoin issuers. In this paper, we adopt the U.S. regulatory framework as our primary reference point for modeling purposes. This approach is motivated by several factors: the maturity and transparency of U.S. financial regulation, its substantial global influence, and the availability of comprehensive legislative proposals such as the GENIUS Act. While our analysis focuses on U.S. regulations, the resulting models readily generalize to other jurisdictions, as most major economies have converged on similar regulatory principles for stablecoins—particularly the requirements for full collateralization through high-quality liquid assets and robust redemption guarantees. Under the U.S. regulatory framework, Title VII, Section 604(b)(1) of the Guiding and Establishing National Innovation for U.S. Stablecoins Act of 2025 (the "GENIUS Act") delineates six categories of high-quality, liquid assets eligible to serve as collateral for payment stablecoins on a strict 1:1 basis [1]:

- (1) **U.S. currency and balances held directly at a Federal Reserve Bank**
- (2) **Demand deposits at FDIC-insured depository institutions**; that is, checking or transaction accounts held at commercial banks, insured by the U.S. government against default.
- (3) **U.S. Treasury securities with residual maturity ≤ 90 days**; that is, short-term federal debt instruments.
- (4) **Overnight reverse-repo agreements backed by Treasuries, cleared tri-party or with a highly credit-worthy counterparty**; i.e., short-term lending arrangements where the issuer temporarily exchanges cash for Treasury collateral, typically settled via a clearing bank.
- (5) **Government-only money-market fund shares invested solely in assets (1)–(4)**; that is, pooled investment vehicles offering liquidity and diversification while limiting holdings to ultra-safe, short-term instruments.
- (6) **Tokenised forms of any asset in (1)–(5), excluding repo contracts**; that is, cryptographic representations of reserve assets issued on a blockchain, provided the underlying remains fully redeemable and auditable.

These six categories establish a natural liquidity hierarchy that reflects different settlement windows and operational characteristics. At the apex of this hierarchy are cash balances and Federal Reserve master accounts, which provide instantaneous settlement capability but generate no yield, creating an inflation drag on reserves while offering complete elimination of market risk. Shortterm U.S. Treasury securities with maturities of 90 days or less generally settle within standard banking hours, providing substantially higher yields that currently approximate 5.4% p.a. while maintaining deep market liquidity and qualifying as Level-1 High Quality Liquid Assets under Basel III regulations. However, these instruments introduce duration risk and potential fire-sale losses during periods of intense redemption pressure. The remaining asset classes

exhibit varying combinations of liquidity constraints and settlement windows that create a graduated spectrum of operational flexibility. FDIC-insured demand deposits typically process during Fedwire operating windows, while government money market fund shares offer same-day liquidity under normal market conditions but may impose restrictions during periods of market stress. Tokenized representations of these assets provide 24/7 trading capability through blockchain networks, though final settlement of the wrapped asset remains constrained by the operational windows of the native market.

The fundamental trade-off between cash and Treasury securities illustrates the central tension in stablecoin reserve management. Cash holdings maximize liquidity and eliminate market risk but impose opportunity costs through foregone interest income, particularly pronounced in rising rate environments. Treasury securities offer attractive risk-adjusted returns and maintain high liquidity under normal conditions but introduce duration risk and volatility during market dislocations. The other permitted asset classes present similar risk-return considerations, each with specific additional complexities such as smart contract and legal title risks introduced by tokenized wrappers.

Throughout our analysis, we adopt benchmark parameters that reflect current market conditions, with the risk-free cash rate set at zero as vault cash earns no interest, while three-month Treasury securities yield approximately 5.4% p.a. based on prevailing yield curves.¹

2.2. A Dynamic Reserve Model

2.2.1. Demand And Peg Stability

The peg deviation $\Delta P(t) \in \mathbb{R}$ measures the stablecoin's price displacement from its \$1 target, where $\Delta P(t) > 0$ indicates the coin trades below par. We model the stablecoin's mint and redemption dynamics as self-exciting processes that capture the empirical tendency for large transactions to cluster in time, while the peg deviation evolves deterministically based on liquidity shortfalls. Let $N_R(t)$ and $N_M(t)$ denote the cumulative redemption and mint counts up to time t , each following a univariate Hawkes process with stochastic intensities

$$\lambda_R(t) = \lambda_{0,R} + \int_0^t \kappa_R e^{-\theta_R(t-s)} dN_R(s) + \zeta \Delta P(t), \quad (1)$$

$$\lambda_M(t) = \lambda_{0,M} + \int_0^t \kappa_M e^{-\theta_M(t-s)} dN_M(s), \quad (2)$$

where $\lambda_{0,R}, \lambda_{0,M} \geq 0$ are baseline intensities, $\kappa_R, \kappa_M > 0$ capture self-excitation (each event increases the likelihood of subsequent events), and $\theta_R, \theta_M > 0$ govern the exponential decay of this excitation. The redemption intensity includes an additional feedback term $\zeta \Delta P(t)^2$ with $\zeta \geq 0$, reflecting how peg instability accelerates redemptions. This mechanism endogenously models bank-run dynamics characterized by self-reinforcing distrust in the currency's stability.

Let $M(t)$ and $R(t)$ denote cumulative dollar volumes of mints and redemptions, with instantaneous net redemption flow $Q(t) = \dot{R}(t) - \dot{M}(t)$. These dollar flows arise

¹Indicative annualized yields as of 2Aug2025.

from the counting processes via marked point process representations:

$$dR(t) = \int_{\mathbb{R}_+} z N_R(dt, dz), \quad dM(t) = \int_{\mathbb{R}_+} z N_M(dt, dz), \quad (3)$$

where marks z represent individual transaction sizes with finite first moments.

The peg deviation evolves deterministically according to unmet redemption demand relative to outstanding supply:

$$\frac{d}{dt} \Delta P(t) = \eta \frac{[Q(t) - R_{\text{liq}}(t)]_+}{S_{\text{out}}(t)} - \gamma \delta(t), \quad (4)$$

where $R_{\text{liq}}(t)$ denotes immediately available cash reserves, $S_{\text{out}}(t) = S_{\text{out}}(0) + M(t) - R(t)$ is the outstanding supply, and $\delta(t)$ represents the mint/burn fee spread. The deviations resulting from equation (4) directly reflect deficits in reserve coverage, rather than being mitigated by supply and demand. The first term captures how liquidity shortfalls—when redemption requests $Q(t)$ exceed available cash $R_{\text{liq}}(t)$ —create peg pressure proportional to the fraction of supply that cannot be serviced. The parameter $\eta > 0$ governs this sensitivity, while $\gamma > 0$ determines how effectively fees can counteract peg deviations. This deterministic relationship makes peg stability an operational challenge: maintaining $\Delta P(t) \approx 0$ requires either sufficient liquidity buffers or appropriate fee policies to offset redemption pressure.

2.2.2. Reserve-Balance State Model

In the remaining text, we make the simplifying assumption that the coin issuer employs only vault cash (categories 1-2 from subsection 2.1) and short-dated Treasury securities (category 3) as reserve assets. This simplification is due to the fact that the remaining permitted asset types primarily represent overnight carries or swaps of these two base assets, serving as operational vehicles rather than fundamentally distinct reserve instruments. The stablecoin issuer's operational challenge involves dynamically allocating reserves between immediately available cash and yield-bearing Treasury securities while maintaining peg stability. We formalize this as a control problem with state vector

$$x(t) = \begin{bmatrix} R_{\text{liq}}(t) \\ R_{\text{bill}}(t) \\ \Delta P(t) \\ \lambda_R(t) \\ \lambda_M(t) \end{bmatrix}, \quad (5)$$

where $R_{\text{liq}}(t)$ represents immediately available cash reserves, $R_{\text{bill}}(t)$ denotes the face value of short-dated Treasury securities, $\Delta P(t)$, and $\lambda_R(t)$, $\lambda_M(t)$ are the Hawkes intensities governing redemption and mint clustering. The controller manages this system through

$$u(t) = \begin{bmatrix} \omega(t) \\ \delta(t) \end{bmatrix} \in [-\omega_{\max}, \omega_{\max}] \times [-\delta_{\max}, \delta_{\max}], \quad (6)$$

where $\omega(t)$ represents the reallocation flow between cash and bills (positive for cash-to-bills, negative for bills-to-cash), and $\delta(t)$ is the mint/burn fee spread.

The reserve balances evolve according to

$$dR_{\text{liq}}(t) = r_{\text{cash}} R_{\text{liq}}(t) dt - Q(t) dt - \omega(t) dt, \quad (7)$$

$$dR_{\text{bill}}(t) = r_{\text{bill}}(t) R_{\text{bill}}(t) dt + \omega(t) dt. \quad (8)$$

For tractability within control horizons $[t_k, t_{k+1}]$, we treat the T-bill rate as piecewise constant: $r_{\text{bill}}(t) \equiv r_{\text{bill}}^{(k)}$ for $t \in [t_k, t_{k+1}]$. Our baseline assumes $r_{\text{cash}} = 0$, reflecting that vault cash and Federal Reserve master account balances earn no interest, though the framework accommodates $r_{\text{cash}} \neq 0$ without structural changes.

The state constraints $R_{\text{liq}}(t) \geq 0$ and $R_{\text{bill}}(t) \geq 0$, combined with the bounded reallocation rate $|\omega(t)| \leq \omega_{\max}$, endogenize the fundamental liquidity-yield trade-off: higher Treasury allocations increase returns but reduce the buffer against redemption surges, potentially triggering peg instability through the mechanism in equation (4). The balance sheet identity $R_{\text{liq}}(t) + R_{\text{bill}}(t) = S_{\text{out}}(t)$ (up to small operational items) ensures conservation of reserves relative to outstanding supply.

2.2.3. Optimal Control Problem

The stablecoin issuer seeks to maximize yield while maintaining peg stability and operational efficiency. We formalize this through a cost functional that captures the competing objectives of interest generation, peg quality, user experience, and operational frictions. The instantaneous cost is

$$\ell(x(t), u(t)) = c_{\text{peg}} \Delta P(t)^2 + c_{\text{fee}} \delta(t)^2 + \lambda_{\omega} |\omega(t)| + \frac{1}{2} \rho_{\omega} \omega(t)^2 - r_{\text{bill}}^{(k)} R_{\text{bill}}(t), \quad (9)$$

where the terms represent: (i) peg stability penalty $c_{\text{peg}} \Delta P(t)^2$ monetizing reputational and convertibility risks from price deviations; (ii) fee friction $c_{\text{fee}} \delta(t)^2$ discouraging excessive mint/burn spreads that degrade user experience; (iii) reallocation cost $\lambda_{\omega} |\omega(t)| + \frac{1}{2} \rho_{\omega} \omega(t)^2$ capturing operational frictions and market impact from portfolio adjustments; and (iv) interest benefit $-r_{\text{bill}}^{(k)} R_{\text{bill}}(t)$ representing carry from Treasury holdings. The quadratic penalties ensure convexity while the linear yield term creates the fundamental tension between liquidity provision and return generation.

The infinite-horizon stochastic optimal control problem is to select an admissible control process $u(\cdot) = (\omega(\cdot), \delta(\cdot))$ minimizing the expected discounted cost:

$$J_{\infty}(x(0)) = \min_{u(\cdot) \in \mathcal{U}} \mathbb{E} \left[\int_0^{\infty} e^{-\rho t} \ell(x(t), u(t)) dt \right], \quad (10)$$

subject to the system dynamics

$$dR_{\text{liq}}(t) = r_{\text{cash}}R_{\text{liq}}(t)dt - Q(t)dt - \omega(t)dt, \quad (11)$$

$$dR_{\text{bill}}(t) = r_{\text{bill}}^{(k)}R_{\text{bill}}(t)dt + \omega(t)dt, \quad (12)$$

$$\dot{\Delta P}(t) = \eta \frac{[Q(t) - R_{\text{liq}}(t)]_+}{S_{\text{out}}(t)} - \gamma \delta(t), \quad (13)$$

$$d\lambda_R(t) = -\theta_R(\lambda_R(t) - \lambda_{0,R})dt + \kappa_R dN_R(t) + \zeta \Delta P(t)^2 dt, \quad (14)$$

$$d\lambda_M(t) = -\theta_M(\lambda_M(t) - \lambda_{0,M})dt + \kappa_M dN_M(t), \quad (15)$$

where the net redemption flow $Q(t) = \dot{R}(t) - \dot{M}(t)$ arises from marked Hawkes processes with intensities $\lambda_R(t)$, $\lambda_M(t)$ and trade-size marks of finite first moment.

Admissible controls must satisfy the operational constraints (6), be progressively measurable with respect to the filtration $\{\mathcal{F}_t\}$, and maintain state feasibility $R_{\text{liq}}(t), R_{\text{bill}}(t) \geq 0$.

The infinite-horizon problem faces well-posedness challenges from cost integral convergence despite potentially unbounded Treasury growth, the non-smooth term $[Q(t) - R_{\text{liq}}(t)]_+$ in peg dynamics, and potentially explosive paths from the peg-redemption feedback loop. The following standard conditions ensure well-posedness: (i) positive discount rate $\rho > 0$ with bounded interest rates; (ii) subcritical Hawkes processes satisfying $\kappa_R/\theta_R < 1$ and $\kappa_M/\theta_M < 1$ ensuring stationary intensities; (iii) bounded controls maintaining nonnegative reserves; and (iv) the balance sheet constraint preventing unbounded carry extraction.

3. Analytical and Computational Methods

3.1. Stochastic Model Predictive Control

The infinite-horizon optimal control problem formulated above presents significant computational challenges for real-time implementation. This motivates our adoption of Model Predictive Control (MPC), a rolling optimization strategy that approximates the infinite-horizon solution through repeated finite-period problems. Model Predictive Control implements the following strategy: at each decision time t_k , we solve a finite-horizon optimal control problem using the current state and forecasts of future uncertainty. Only the initial portion of the computed optimal trajectory is implemented before re-solving at the next decision point t_{k+1} with updated information. This approach naturally handles constraints while incorporating predictions of future system behavior. For stablecoin reserve management, MPC offers several key advantages: it requires no prior training data, making it immediately applicable without extensive historical datasets; it produces transparent and auditable policies through explicit optimization of well-defined objectives, ensuring regulatory compliance; it naturally incorporates forward-looking capability to anticipate redemption clusters and settlement windows; and it effectively handles high-dimensional continuous state spaces and hybrid jump dynamics through direct optimization.

At each roll time t_k , we solve the finite-horizon stochastic optimal control problem

$$\min_{u(\cdot) \in \mathcal{U}} J_k = \mathbb{E} \left[\int_{t_k}^{t_k+T} e^{-\rho(t-t_k)} \ell(x(t), u(t)) dt \mid \mathcal{F}_{t_k} \right] \quad (16)$$

subject to the system dynamics and admissibility constraints. The filtration \mathcal{F}_{t_k} represents all information available at time t_k , including the complete history of mint and redemption events, current reserve levels, and realized peg deviations. As a measure-theoretic object, \mathcal{F}_{t_k} is the σ -algebra generated by all observable processes up to time t_k , ensuring that our control decisions are non-anticipating—they depend only on past and present information, not future realizations.

Our stochastic MPC framework reduces the stochastic optimization problem to a deterministic equivalent through moment-based approximation of the underlying stochastic processes. Rather than propagating full probability distributions or sampling scenarios, we replace all random quantities by their conditional expectations given \mathcal{F}_{t_k} . This transformation occurs at two levels. First, between MPC rolls, we maintain filtered estimates of the Hawkes intensities using the recursive updates

$$\lambda_X(t^+) = \lambda_X(t^-) + \kappa_X \quad (\text{at event}), \quad (17)$$

$$\lambda_X(t + \Delta)^- = \lambda_{0,X} + (\lambda_X(t^+) - \lambda_{0,X})e^{-\theta_X \Delta} \quad (\text{between events}). \quad (18)$$

for $X \in \{R, M\}$. These updates are deterministic given the observed event stream, providing initial conditions $\lambda_R(t_k^+)$ and $\lambda_M(t_k^+)$ for the planning phase.

Within the optimization horizon $[t_k, t_k + T]$, we must propagate conditional mean intensities to compute the expected redemption flow $\hat{Q}(t)$ at each instant. Simply using initial intensities would ignore the predictable evolution of redemption pressure over the planning horizon. The conditional mean intensities evolve according to

$$\dot{\hat{\lambda}}_R(t) = -\theta_R(\hat{\lambda}_R(t) - \lambda_{0,R}) + \kappa_R \hat{\lambda}_R(t) + \zeta \Delta P(t)^2, \quad \hat{\lambda}_R(t_k) = \lambda_R(t_k^+), \quad (19)$$

$$\dot{\hat{\lambda}}_M(t) = -\theta_M(\hat{\lambda}_M(t) - \lambda_{0,M}) + \kappa_M \hat{\lambda}_M(t), \quad \hat{\lambda}_M(t_k) = \lambda_M(t_k^+), \quad (20)$$

where the self-excitation terms $\kappa_X \hat{\lambda}_X(t)$ arise from taking expectations of future jump contributions. These ODEs exploit the Markovian property of exponential Hawkes processes: given current intensities, the expected future evolution depends only on these values, not the full history. The expected net redemption flow $\hat{Q}(t) = \bar{z}_R \hat{\lambda}_R(t) - \bar{z}_M \hat{\lambda}_M(t)$ then enters the deterministic system dynamics, with the crucial feedback that peg deviations influence future redemption intensity through the $\zeta \Delta P(t)^2$ term. This coupling necessitates joint propagation of all state variables, as flows and peg trajectory depend on each other dynamically. Given mean transaction sizes \bar{z}_R and \bar{z}_M , the expected net redemption flow becomes $\hat{Q}(t) = \bar{z}_R \hat{\lambda}_R(t) - \bar{z}_M \hat{\lambda}_M(t)$. Substituting these deterministic forecasts into the system dynamics yields

$$\dot{R}_{\text{liq}}(t) = r_{\text{cash}} R_{\text{liq}}(t) - \hat{Q}(t) - \omega(t), \quad (21)$$

$$\dot{R}_{\text{bill}}(t) = r_{\text{bill}}^{(k)} R_{\text{bill}}(t) + \omega(t), \quad (22)$$

$$\dot{\Delta P}(t) = \eta \frac{[\hat{Q}(t) - R_{\text{liq}}(t)]_+}{\hat{S}_{\text{out}}(t)} - \gamma \delta(t), \quad (23)$$

where $\hat{S}_{\text{out}}(t)$ evolves according to the expected mint and redemption flows. The computed trajectory $u^*(t)$ for $t \in [t_k, t_k + T]$ represents the optimal response to expected future conditions, with only the initial segment $u^*(t)$ for $t \in [t_k, t_{k+1})$ implemented before re-solving with updated state information.

3.2. Event-Triggered Optimization via Pontryagin's Maximum Principle

Within each MPC roll, we solve the deterministic surrogate problem obtained by replacing stochastic flows with their conditional expectations. The state vector $x = (R_{\text{liq}}, R_{\text{bill}}, \Delta P)^\top$ evolves according to the moment-closed dynamics from Section 3.1, while the Hawkes intensities $\hat{\lambda}_R, \hat{\lambda}_M$ enter as exogenous trajectories.

We seek an optimal control trajectory $u(\cdot)$ from a suitable function space, such as the Banach space of square-integrable functions $L^2([0, T], \mathbb{R}^m)$, rather than a finite-dimensional vector. This makes the optimization problem infinite-dimensional. To solve the optimal control problem, Pontryagin's Maximum Principle (PMP) transforms the dynamic optimization into a system of differential equations. The optimal control at each instant must minimize the current-value Hamiltonian

$$H = \ell(x, u) + p^\top f(x, u, t), \quad (24)$$

which captures the total instantaneous cost: the direct running cost $\ell(x, u)$ plus the marginal effect of the control on future costs through its impact on state evolution $f(x, u, t)$. The optimal control thus balances immediate costs against future consequences. The costates $p = (p_{\text{liq}}, p_{\text{bill}}, p_{\Delta P})^\top$ can consequently be interpreted as shadow prices or marginal values of the state variables, measuring how a unit change in each state affects the total objective value going forward.

Following Pontryagin's Maximum Principle for infinite-horizon problems, the optimal trajectory must satisfy the following canonical equations:

$$\dot{x}^* = f(x^*, u^*, t), \quad x^*(0) = x_0, \quad (25)$$

$$\dot{p} = \rho p - \nabla_x H(x^*, u^*, p, t), \quad (26)$$

$$u^*(t) \in \arg \min_{u \in \mathcal{U}} H(x^*(t), u, p(t), t), \quad (27)$$

where the first term in (26) reflects the accumulation of shadow costs at the discount rate, while the second term accounts for their depletion as costs are realized over the infinitesimal interval $[t, t + dt]$. The transversality condition $\lim_{t \rightarrow \infty} e^{-\rho t} p^\top(t) x^*(t) = 0$ ensures that the discounted value of the terminal state vanishes, preventing unbounded growth of the state-costate product. Since our cost functional is convex in controls and the reserve dynamics are affine, these necessary conditions from PMP are also sufficient for optimality, guaranteeing that any solution to this system is globally optimal.

The costate dynamics yield explicit expressions for the shadow prices. For the current-value Hamiltonian

$$\begin{aligned} H = & c_{\text{peg}} \Delta P^2 + c_{\text{fee}} \delta^2 + \lambda_\omega |\omega| + \frac{1}{2} \rho_\omega \omega^2 - r_{\text{bill}} R_{\text{bill}} \\ & + p_{\text{liq}} (r_{\text{cash}} R_{\text{liq}} - \hat{Q} - \omega) + p_{\text{bill}} (r_{\text{bill}} R_{\text{bill}} + \omega) \\ & + p_{\Delta P} \left(\eta \frac{[\hat{Q} - R_{\text{liq}}]_+}{\hat{S}_{\text{out}}} - \gamma \delta \right), \end{aligned} \quad (28)$$

the costates satisfy (almost everywhere at points where $R_{\text{liq}} \neq \hat{Q}$)

$$\dot{p}_{\text{liq}} = \rho p_{\text{liq}} - \frac{\partial H}{\partial R_{\text{liq}}} = \rho p_{\text{liq}} - \left(p_{\text{liq}} r_{\text{cash}} - p_{\Delta P} \eta \frac{\mathbf{1}_{\{\hat{Q} > R_{\text{liq}}\}}}{\hat{S}_{\text{out}}} \right), \quad (29)$$

$$\dot{p}_{\text{bill}} = \rho p_{\text{bill}} - \frac{\partial H}{\partial R_{\text{bill}}} = \rho p_{\text{bill}} - (-r_{\text{bill}} + p_{\text{bill}} r_{\text{bill}}) = (\rho - r_{\text{bill}}) p_{\text{bill}} + r_{\text{bill}}, \quad (30)$$

$$\dot{p}_{\Delta P} = \rho p_{\Delta P} - \frac{\partial H}{\partial \Delta P} = \rho p_{\Delta P} - 2c_{\text{peg}} \Delta P, \quad (31)$$

where $\mathbf{1}_{\{\hat{Q} > R_{\text{liq}}\}}$ is the indicator function that equals 1 when redemptions exceed liquid reserves and 0 otherwise.

The first-order conditions for control optimality yield

$$0 \in \partial_{\omega} H = \lambda_{\omega} \partial |\omega| + \rho_{\omega} \omega - p_{\text{liq}} + p_{\text{bill}}, \quad (32)$$

$$0 = \frac{\partial H}{\partial \delta} = 2c_{\text{fee}} \delta - \gamma p_{\Delta P}. \quad (33)$$

Thus, the fee control admits the linear feedback law

$$\delta^*(t) = \text{Proj}_{[-\delta_{\max}, \delta_{\max}]} \left(\frac{\gamma}{2c_{\text{fee}}} p_{\Delta P}(t) \right), \quad (34)$$

where projection operator $\text{Proj}_{[a,b]}(\cdot)$ clips values to the constraint interval. The reallocation control exhibits more sophisticated structure due to the ℓ_1 trading cost (the $\lambda_{\omega} |\omega|$ term).

Define the switching function

$$S_{\omega}(t) = p_{\text{bill}}(t) - p_{\text{liq}}(t), \quad (35)$$

which represents the instantaneous net opportunity cost of holding bills rather than cash. Solving the stationarity condition (32) for $\omega(t)$ yields

$$\omega^*(t) = \text{Proj}_{[-\omega_{\max}, \omega_{\max}]} \left(-\frac{1}{\rho_{\omega}} \text{shrink}(S_{\omega}(t), \lambda_{\omega}) \right), \quad (36)$$

where $\text{shrink}(z, \lambda) = \text{sign}(z) \max\{|z| - \lambda, 0\}$ denotes the soft-thresholding operator. This implies that the optimal portfolio reallocation control ω at time t follows a *threshold policy*: if the absolute marginal benefit of reallocation does not exceed the transaction cost ($|S_{\omega}(t)| \leq \lambda_{\omega}$), no reallocation within the reserve asset portfolio occurs ($\omega^*(t) = 0$). If the marginal benefit exceeds the transaction cost ($|S_{\omega}(t)| > \lambda_{\omega}$), reallocation is performed at the maximal admissible rate ($\omega^*(t) \in \{-\omega_{\max}, \omega_{\max}\}$).

3.3. Implementation with Settlement Windows

3.3.1. A Discretized Optimal Control Policy

The continuous-time event-triggered policy, while theoretically elegant, requires potential control updates at every mint or redemption event—impractical given typical

transaction volumes. We therefore develop a sampled-data formulation that aligns with operational realities and provides computational tractability.

Let $0 = \tau_0 < \tau_1 < \tau_2 < \dots$ denote predetermined settlement or review times (e.g., Fedwire windows, hourly desk reviews) with intervals $\Delta_j = \tau_{j+1} - \tau_j$. We constrain controls to be piecewise constant over these windows:

$$\omega(t) \equiv \omega_j, \quad \delta(t) \equiv \delta_j \quad \text{for } t \in [\tau_j, \tau_{j+1}). \quad (37)$$

This restriction reflects a real operational constraint, as treasury trades typically execute in batches at settlement windows, and defines the admissible control set \mathcal{U}_{sd} .

Within this framework, the Hamiltonian contribution from reallocation over window j becomes

$$\int_{\tau_j}^{\tau_{j+1}} (\lambda_\omega |\omega_j| + \frac{1}{2} \rho_\omega \omega_j^2 - (p_{\text{bill}}(t) - p_{\text{liq}}(t)) \omega_j) dt. \quad (38)$$

Define

$$S_j := \int_{\tau_j}^{\tau_{j+1}} (p_{\text{bill}}(t) - p_{\text{liq}}(t)) dt, \quad (39)$$

which represents the accumulated relative value of bills versus cash over the window.

Theorem 3.1 (Window-Based Optimal Control). *The optimal sampled-data controls over window j are:*

$$\omega_j^* = \text{Proj}_{[-\omega_{\max}, \omega_{\max}]} \left(-\frac{1}{\rho_\omega \Delta_j} \text{shrink}(S_j, \lambda_\omega \Delta_j) \right), \quad (40)$$

$$\delta_j^* = \text{Proj}_{[-\delta_{\max}, \delta_{\max}]} \left(\frac{\gamma}{2c_{\text{fee}}} \frac{1}{\Delta_j} \int_{\tau_j}^{\tau_{j+1}} p_{\Delta P}(t) dt \right), \quad (41)$$

where $\text{shrink}(z, \lambda) = \text{sign}(z) \max\{|z| - \lambda, 0\}$.

Proof. We need to minimize over window j the functional

$$J_j(\omega_j) = \int_{\tau_j}^{\tau_{j+1}} (\lambda_\omega |\omega_j| + \frac{1}{2} \rho_\omega \omega_j^2 - (p_{\text{bill}}(t) - p_{\text{liq}}(t)) \omega_j) dt \quad (42)$$

subject to $\omega_j \in [-\omega_{\max}, \omega_{\max}]$. Since ω_j is constant over $[\tau_j, \tau_{j+1})$, we can factor it out:

$$J_j(\omega_j) = \lambda_\omega \Delta_j |\omega_j| + \frac{1}{2} \rho_\omega \Delta_j \omega_j^2 - S_j \omega_j, \quad (43)$$

where $S_j = \int_{\tau_j}^{\tau_{j+1}} (p_{\text{bill}}(t) - p_{\text{liq}}(t)) dt$ as defined in (39).

First consider the unconstrained problem. The objective is convex (sum of convex functions), and strictly convex when $\rho_\omega > 0$ since the Hessian $\nabla^2 J_j = \rho_\omega \Delta_j > 0$.

For optimality, we require $0 \in \partial J_j(\omega_j)$, where ∂ denotes the subdifferential. Computing term by term:

- $\partial_{\omega_j} [\frac{1}{2} \rho_\omega \Delta_j \omega_j^2] = \rho_\omega \Delta_j \omega_j$
- $\partial_{\omega_j} [-S_j \omega_j] = -S_j$

- $\partial_{\omega_j}[\lambda_\omega \Delta_j |\omega_j|] = \lambda_\omega \Delta_j \cdot \partial |\omega_j|$

For the absolute value subdifferential at point ω_j :

$$\partial |\omega_j| = \begin{cases} \{1\} & \text{if } \omega_j > 0 \\ \{-1\} & \text{if } \omega_j < 0 \\ [-1, 1] & \text{if } \omega_j = 0 \end{cases} \quad (44)$$

Therefore, the optimality condition $0 \in \partial J_j(\omega_j)$ becomes:

$$0 \in \lambda_\omega \Delta_j \cdot \partial |\omega_j| + \rho_\omega \Delta_j \omega_j - S_j. \quad (45)$$

We analyze three cases:

Case 1: $\omega_j > 0$. Then $\partial |\omega_j| = \{1\}$, so:

$$0 = \lambda_\omega \Delta_j + \rho_\omega \Delta_j \omega_j - S_j \implies \omega_j = \frac{S_j - \lambda_\omega \Delta_j}{\rho_\omega \Delta_j}. \quad (46)$$

This is valid only if $\omega_j > 0$, i.e., when $S_j > \lambda_\omega \Delta_j$.

Case 2: $\omega_j < 0$. Then $\partial |\omega_j| = \{-1\}$, so:

$$0 = -\lambda_\omega \Delta_j + \rho_\omega \Delta_j \omega_j - S_j \implies \omega_j = \frac{S_j + \lambda_\omega \Delta_j}{\rho_\omega \Delta_j}. \quad (47)$$

This is valid only if $\omega_j < 0$, i.e., when $S_j < -\lambda_\omega \Delta_j$.

Case 3: $\omega_j = 0$. Then $\partial |\omega_j| = [-1, 1]$, so we need:

$$0 \in \lambda_\omega \Delta_j [-1, 1] + 0 - S_j = [-\lambda_\omega \Delta_j - S_j, \lambda_\omega \Delta_j - S_j]. \quad (48)$$

This holds if and only if $-\lambda_\omega \Delta_j \leq S_j \leq \lambda_\omega \Delta_j$, i.e., $|S_j| \leq \lambda_\omega \Delta_j$.

Combining all cases, the unconstrained optimizer is:

$$\omega_j^{\text{unc}} = \begin{cases} \frac{S_j - \lambda_\omega \Delta_j}{\rho_\omega \Delta_j} & \text{if } S_j > \lambda_\omega \Delta_j \\ 0 & \text{if } |S_j| \leq \lambda_\omega \Delta_j \\ \frac{S_j + \lambda_\omega \Delta_j}{\rho_\omega \Delta_j} & \text{if } S_j < -\lambda_\omega \Delta_j \end{cases} \quad (49)$$

This can be written compactly using the soft-thresholding operator:

$$\omega_j^{\text{unc}} = -\frac{1}{\rho_\omega \Delta_j} \text{shrink}(S_j, \lambda_\omega \Delta_j), \quad (50)$$

where $\text{shrink}(z, \lambda) := \text{sign}(z) \max\{|z| - \lambda, 0\}$.

The constraint set $[-\omega_{\max}, \omega_{\max}]$ is closed and convex. Since J_j is strictly convex, the constrained minimizer is unique and given by the Euclidean projection:

$$\omega_j^* = \text{Proj}_{[-\omega_{\max}, \omega_{\max}]}(\omega_j^{\text{unc}}) = \text{Proj}_{[-\omega_{\max}, \omega_{\max}]} \left(-\frac{1}{\rho_\omega \Delta_j} \text{shrink}(S_j, \lambda_\omega \Delta_j) \right), \quad (51)$$

which completes the proof. \square

This result preserves the essential structure of the continuous-time solution while offering practical advantages. Control decisions require only time-averaged costates S_j and $\bar{p}_{\Delta P, j}$, computed once per settlement window rather than at each transaction, reducing computational complexity from potentially thousands of transactions to typically 6-24 daily windows. The policy naturally aligns with institutional constraints by executing treasury transactions at predetermined windows matching market infrastructure like Fedwire hours and repo settlement times, while the averaged switching function S_j smooths intra-window flow volatility to prevent overreaction to temporary imbalances. The decision rule admits a transparent interpretation: rebalance at each window if the averaged value differential exceeds the transaction cost threshold $\lambda_\omega \Delta_j$, otherwise maintain positions. Moreover, the effective inaction threshold automatically adapts to operating conditions, scaling with window length to allow more aggressive rebalancing over longer intervals where costs amortize better, while becoming more conservative during stress periods with frequent reviews.

3.3.2. Monotone Stress-Response Behavior

In this section, we analyze how the window-based optimal control responds to varying levels of redemption pressure. The system favors yield-bearing Treasury holdings during calm periods and shifts toward cash as redemption demand intensifies. The following theorem establishes this behavior through analysis of the costate dynamics:

Theorem 3.2 (Monotone Stress-Threshold Principle). *Consider the window-based optimal control (40) over interval $[\tau_j, \tau_{j+1}]$. Let $\hat{Q}^{(1)}$ and $\hat{Q}^{(2)}$ be two forecast paths with $\hat{Q}^{(1)}(t) \geq \hat{Q}^{(2)}(t)$ for all $t \in [\tau_j, \tau_{j+1}]$. Then:*

- (1) *The optimal reallocation satisfies $\omega_j^*(\hat{Q}^{(1)}) \leq \omega_j^*(\hat{Q}^{(2)})$*
- (2) *For any parametric family $\hat{Q}_\alpha(t) = \alpha q(t)$ with $q(t) \geq 0$, there exists a threshold $\alpha^* \geq 0$ such that:*

$$\omega_j^*(\hat{Q}_\alpha) = \begin{cases} 0 & \text{if } \alpha \leq \alpha^* \\ \in \{-\omega_{\max}, 0, +\omega_{\max}\} & \text{if } \alpha > \alpha^* \end{cases} \quad (52)$$

- (3) *As $\alpha \rightarrow \infty$, $\omega_j^*(\hat{Q}_\alpha) \rightarrow -\omega_{\max}$ (maximum cash building)*

Proof. We establish monotonicity through a sequence of comparison results on the state-costate system.

Step 1: State monotonicity. Under fixed controls (ω_j, δ_j) and identical initial conditions, the state dynamics yield:

$$\frac{d}{dt} [R_{\text{liq}}^{(1)} - R_{\text{liq}}^{(2)}] = -[\hat{Q}^{(1)} - \hat{Q}^{(2)}] \leq 0, \quad (53)$$

implying $R_{\text{liq}}^{(1)}(t) \leq R_{\text{liq}}^{(2)}(t)$ for all $t \in [\tau_j, \tau_{j+1}]$.

For the peg deviation, since $[\cdot]_+$ is monotone increasing and $\hat{Q}^{(1)} - R_{\text{liq}}^{(1)} \geq \hat{Q}^{(2)} - R_{\text{liq}}^{(2)}$:

$$\Delta \dot{P}^{(1)} - \Delta \dot{P}^{(2)} = \eta \frac{[\hat{Q}^{(1)} - R_{\text{liq}}^{(1)}]_+ - [\hat{Q}^{(2)} - R_{\text{liq}}^{(2)}]_+}{\hat{S}_{\text{out}}} \geq 0, \quad (54)$$

yielding $\Delta P^{(1)}(t) \geq \Delta P^{(2)}(t)$.

Step 2: Costate monotonicity. Working backwards from terminal conditions at τ_{j+1} , the variation of constants formula for the peg costate gives:

$$p_{\Delta P}(t) = e^{\rho(t-\tau_{j+1})} p_{\Delta P}(\tau_{j+1}) - 2c_{\text{peg}} \int_t^{\tau_{j+1}} e^{\rho(t-s)} \Delta P(s) ds. \quad (55)$$

Since $\Delta P^{(1)} \geq \Delta P^{(2)}$, we have $p_{\Delta P}^{(1)}(t) \leq p_{\Delta P}^{(2)}(t)$.

For the liquidity costate, the dynamics

$$\dot{p}_{\text{liq}} = (\rho - r_{\text{cash}}) p_{\text{liq}} + \eta \frac{\mathbf{1}_{\{\hat{Q} > R_{\text{liq}}\}}}{\hat{S}_{\text{out}}} p_{\Delta P} \quad (56)$$

form a linear system with monotone coefficient (the indicator function) and monotone forcing (since $p_{\Delta P}^{(1)} \leq p_{\Delta P}^{(2)}$). Hence,

$$\dot{p}_{\text{liq}}^{(1)}(t) \leq \dot{p}_{\text{liq}}^{(2)}(t) \quad \text{for all } t,$$

and, consequently,

$$p_{\text{liq}}^{(1)}(t) \leq p_{\text{liq}}^{(2)}(t) \quad \text{for all } t.$$

The bill costate evolution is independent of \hat{Q} , so $p_{\text{bill}}^{(1)} = p_{\text{bill}}^{(2)}$.

Step 3: Switching function monotonicity. The averaged switching function satisfies:

$$S_j(\hat{Q}^{(1)}) - S_j(\hat{Q}^{(2)}) = \int_{\tau_j}^{\tau_{j+1}} [p_{\text{liq}}^{(2)}(t) - p_{\text{liq}}^{(1)}(t)] dt \geq 0. \quad (57)$$

From (40), the optimal control is:

$$\omega_j^* = \text{Proj}_{[-\omega_{\max}, \omega_{\max}]} \left(-\frac{1}{\rho_{\omega} \Delta_j} \text{shrink}(S_j, \lambda_{\omega} \Delta_j) \right). \quad (58)$$

Since $z \mapsto -\text{shrink}(z, \lambda)$ is monotone decreasing and projection preserves monotonicity, larger S_j yields smaller (more negative) ω_j^* .

For the parametric family $\hat{Q}_{\alpha} = \alpha q$, since $S_j(\hat{Q}_{\alpha})$ is continuous in the forecast path $\hat{Q}_{\alpha}(t)$, it is also continuous in α for $\hat{Q}_{\alpha}(t) = \alpha q(t)$. The threshold structure of the shrinkage operator then guarantees existence of α^* where the control switches from inaction to action. \square

This theorem provides rigorous justification for a simple operational rule:

- **Normal markets** (low α): The optimal policy maintains treasury positions to capture yield
- **Stress onset** ($\alpha \approx \alpha^*$): The system reaches a tipping point where liquidity concerns dominate yield considerations
- **Crisis mode** (high α): The policy aggressively builds cash reserves at maximum feasible rate

The monotonicity property ensures this transition is predictable and one-directional as stress intensifies, preventing rapid switching that could amplify market disruption and erode confidence. This result provides a mathematical formalization of prudent reserve management: Stable markets allow for large positions in interest-bearing T-bonds. With increasing volatility, a significant shift to cash is necessary before sell-offs become self-reinforcing.

4. Numerical Results

In this section, we use simulations of diverse market phenomena to demonstrate the effectiveness of the proposed control algorithm considering both profitability and safety.

4.1. Experimental Design

We conduct numerical experiments over 92 calendar days (August 1 - October 31, 2025) with three daily settlement windows at 10:00, 13:00, and 16:00 ET, aligning with major settlement times. The performance of various control strategies is evaluated using three scenarios that capture characteristic market stress patterns empirically observed in financial markets. The construction of these scenarios enables precise testing of our central hypothesis that the developed control algorithm fulfills three essential requirements: first, the exploitation of lucrative investment opportunities in Treasury Bills during calm market phases; second, the maintenance of sufficient liquidity reserves in volatile phases with potentially endogenous bank-run dynamics; and third, the early detection of emerging volatility phases, such that proactive liquidity procurement is initiated at early signs of a demand shock. To systematically investigate these properties, we define the following market scenarios:

- (1) **Single shock event:** The system operates under baseline conditions for days 0-30, experiences elevated redemption pressure during days 30-45 with baseline intensity $\lambda_{0,R}$ multiplied by a factor $\chi \sim \text{Uniform}[2, 4]$, then undergoes exponential mean-reversion with a 10-day time constant through day 92. This stress test examines the controller's ability to respond decisively to sustained redemption pressure and subsequently restore normalized operations.
- (2) **Prolonged clustering:** The system maintains baseline parameters until day 30. From days 30-70, we increase the self-excitation parameter κ_R equally for both mint and redemption requests to bring the branching ratio κ_R/θ_R to 0.85, approaching criticality. This near-critical regime generates persistent "aftershock" bursts in mints and redemptions that emerge despite normal baseline intensities. After day 70, parameters return to baseline.
- (3) **False alarm (whipsaw):** A brief mint surge occurs during days 30-32 where $\lambda_{0,M}$ triples, followed by a modest redemption increase to $1.5 \times \lambda_{0,R}$ during days 32-35, then returning to baseline. This pattern tests whether the controller avoids unnecessary cash accumulation in response to transient imbalances.

Peg stability is measured by the failure probability, defined as the relative frequency of complete depeg events ($\Delta P = 1$). Responsiveness is measured by the time lag between a shock onset and the controller's increase in cash-buying speed.

In addition to the optimal control described in Subsection 3.3, we evaluate the performance of two reference strategies:

- (1) **The maximum yield strategy:** Maximizes Treasury Bond holdings and converts these to cash exclusively when immediately necessary to cover redemption requests.
- (2) **The maximum liquidity strategy:** Maintains the entire portfolio exclusively in liquid assets.

4.2. Parameter Estimation

The interest rates used in our numerical computations are taken from current yield curves and Federal Reserve projections, expressed on a per-settlement-window basis (8 hours):

- 90-day Treasury rate: $r_{\text{bill}} = 0.054/(3 \times 365) \approx 4.93 \times 10^{-5}$ per window (5.4% annualized yield as of August 2025)
- Discount rate: $\rho = 0.08/(3 \times 365) \approx 7.31 \times 10^{-5}$ per window (8% annualized cost of capital reflecting regulatory risk premium)
- Discount rate: $\rho = 0.08 \times 3/8760 \approx 2.74 \times 10^{-5}$ per window (8% annualized cost of capital reflecting regulatory risk premium)

The following operational parameters are calibrated to approximate those commonly found in industry practices and settlement infrastructure:

- Maximum reallocation rate: $\omega_{\text{max}} = 0.1 \times S_{\text{out}}$ per window (10% of supply)
- Settlement windows: $\Delta_j = 8$ hours (three windows per day)

To simplify the interpretation of numerical results, we assume zero mint or redemption fee ($\delta = 0$). For modelling the Hawkes processes, we choose parameters to mimic the dynamics observed in major stablecoins (USDC, USDT) during 2024-2025. For baseline intensities, we set $\lambda_{0,R} = 100$ events/hour for redemptions and $\lambda_{0,M} = 80$ events/hour for mints, corresponding to daily baseline volumes of 2,400 and 1,920 events respectively, which align with typical median volumes for these assets.

To capture the clustering behavior characteristic of stablecoin transactions, we parameterize the self-excitation dynamics with decay rates of $\theta_R = 2.0 \text{ hour}^{-1}$ and $\theta_M = 1.5 \text{ hour}^{-1}$, yielding half-lives of approximately 20-30 minutes that reflect how quickly bursts of activity dissipate. We set the corresponding jump sizes to $\kappa_R = 0.8$ and $\kappa_M = 0.6$, which ensure subcritical branching ratios ($\kappa_R/\theta_R = 0.4 < 1$ and $\kappa_M/\theta_M = 0.4 < 1$) necessary for process stability. Finally, transaction sizes follow exponential distributions with mean redemption size $\bar{z}_R = \$250,000$ and mean mint size $\bar{z}_M = \$300,000$, values representative of institutional trading volumes in these markets.

The cost function parameters are derived from economic fundamentals and regulatory objectives. For peg stability, we assume that deviations from the dollar peg create arbitrage opportunities proportional to $(\Delta P)^2$. To maintain deviations below 10 basis points under normal conditions, we calibrate the peg stability cost as:

$$c_{\text{peg}} = \frac{\text{Daily carry value}}{\text{Tolerance}^2} = \frac{r_{\text{bill}} \times S_{\text{out}}/365}{(0.001)^2} \approx 1.5 \times 10^8 \quad (59)$$

This ensures that the controller's prioritization of peg maintenance is commensurate with the economic value at stake. The fee penalty parameter balances user experience

with revenue requirements, calibrated to target fees around 10 basis points:

$$c_{\text{fee}} = \frac{\text{Median daily redemption value}}{(\text{Target fee})^2} = \frac{\lambda_{0,R} \times \bar{z}_R \times 24}{(0.01)^2} \approx 6 \times 10^8 \quad (60)$$

Trading costs reflect Treasury market microstructure, with a linear component $\lambda_\omega = 0.0001 \times S_{\text{out}}$ representing the 1 basis point bid-ask spread and a quadratic component $\rho_\omega = 0.00001 \times S_{\text{out}}$ capturing price impact for large trades. The peg dynamics are parameterized based on historical stablecoin de-pegging events: we set the supply-peg sensitivity $\eta = 10$, calibrated so that a 10% supply shortfall creates a 1% peg deviation; the fee effectiveness parameter $\gamma = 5$, whereby a 50 basis point fee counters a 10 basis point deviation; and the peg feedback strength $\zeta = 100$, such that a 1% deviation doubles redemption intensity.

For initial conditions, we consider a system at scale with outstanding supply $S_{\text{out}}(0) = \$10$ billion and zero deviation from the peg ($\Delta P(0) = 0$). Transaction intensities begin at baseline levels: $\lambda_R(0) = \lambda_{0,R}$ and $\lambda_M(0) = \lambda_{0,M}$. The reserve allocation strategies differ between controllers: both the optimal controller and the maximum yield controller begin with $R_{\text{liq}}(0) = \$1$ billion (10%) in liquid assets and $R_{\text{bill}}(0) = \$9$ billion (90%) in Treasury bills, while the maximum liquidity controller starts with all reserves ($\$10$ billion) allocated to liquid cash.

4.3. Presentation Of Results

Revenue is calculated as the negative of the cost functional. Table 1 shows the total revenue by scenario and control strategy. Table 2 displays the fallout rates and responsiveness measures. We simulated 100 scenarios and report average values for all metrics, except for the fallout rate, which is shown as a relative frequency. Figure 1 illustrates the trajectories of the control input ω for all analyzed control strategies and scenarios.

	Strategy	Scenario	Total Revenue
Optimal Control		Single Shock	1.8600×10^8
		Prolonged Clustering	1.2000×10^8
		False Alarm	1.2200×10^8
Maximum Yield		Single Shock	5.5200×10^7
		Prolonged Clustering	3.0100×10^7
		False Alarm	7.8500×10^7
Maximum Liquidity		Single Shock	0.0000
		Prolonged Clustering	0.0000
		False Alarm	0.0000

Table 1. Total Cost by Strategy and Scenario

Strategy	Scenario	Frequency	Resp. (days)
Optimal Control	Single Shock	1.0000	1.75
	Prolonged Clustering	1.0000	2.47
	False Alarm	0.0000	n/a
Maximum Yield	Single Shock	1.0000	0
	Prolonged Clustering	1.0000	0
	False Alarm	1.0000	n/a
Maximum Liquidity	Single Shock	0.0000	n/a
	Prolonged Clustering	0.0000	n/a
	False Alarm	0.0000	n/a

Table 2. Depeg Frequency and Responsiveness

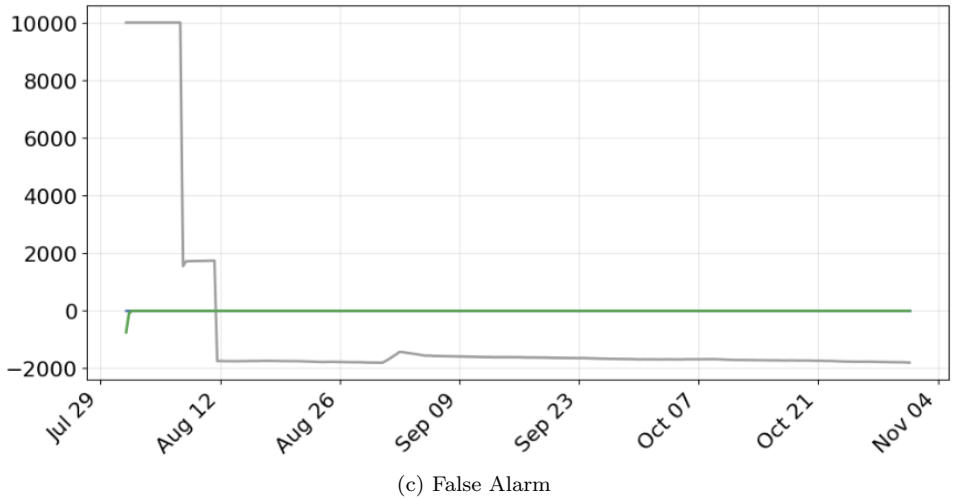
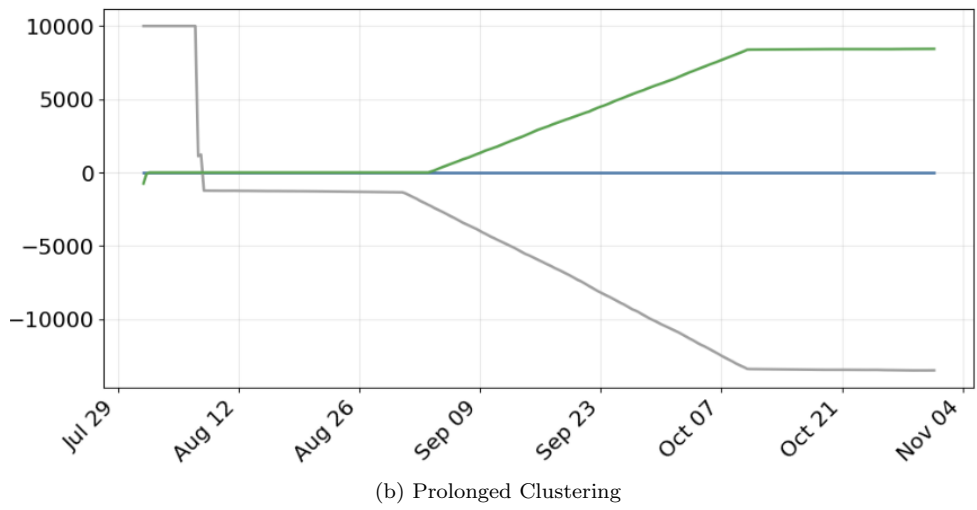
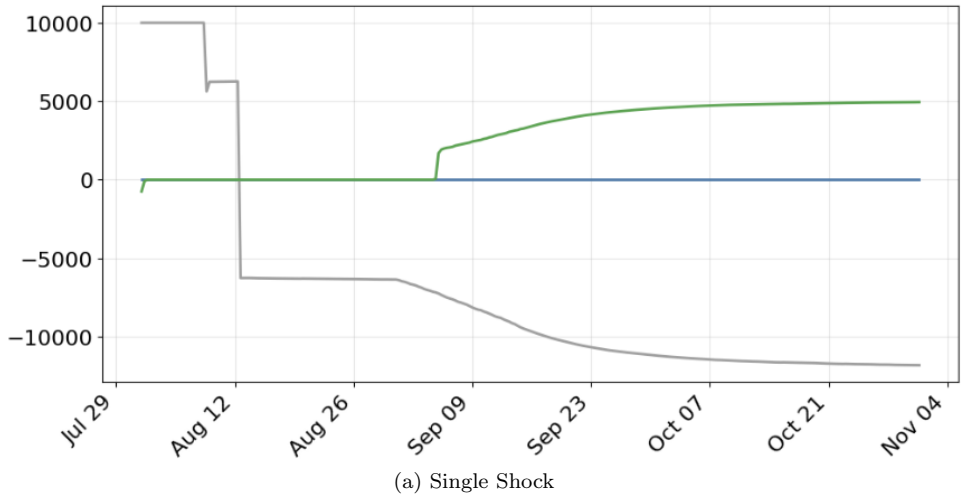


Figure 1. Control actions under different scenarios. The y-axis is scaled in millions dollar per hour. The optimal control is color-coded in green, the maximum-yield strategy in gray, and the maximum-liquidity strategy in blue. The maximum-liquidity strategy initially shifts massively into T-bonds but must later sell these positions to meet redemption requests. The optimal control strategy behaves cautiously at first and increases its T-bond investments only after the stress period. The maximum-yield strategy, by definition, makes no reallocations.

The simulation results demonstrate the significant advantages of the proposed control strategy over both myopic yield maximization (maximum yield strategy) and the conservative cash-only strategy. The maximum yield strategy proves to be clearly inferior: this approach leads to excessive initial bond purchases across all simulated scenarios, and systematically confronts the issuer with high redemption obligations and associated capitalization problems toward the end of the simulation period. Consequently, this strategy exhibits clear underperformance compared to the optimized control both in terms of generated revenue and default rates. The responsiveness of this strategy exceeds that of the the proposed approach, as the maximum yield controller usually already experiences liquidity constraints at the time of shock onset and consequently must react more promptly to increased redemption requests. The advantages of our method over the maximum liquidity strategy are more moderate. However, particularly during the more stable market phase at the end of the simulation period, it becomes evident that larger-volume bond purchases are justifiable. Through this strategic orientation, the optimized controller achieves a significant financial advantage over the conservative strategy.

5. Conclusion

This paper develops an operations-first framework for managing the reserves of a pegged digital currency, accounting for clustering dynamics in order and redemption flows and an endogenous dynamical relationship between peg deviation and redemp-
tion intensities. We represent mints and redemptions as self-exciting point processes and treat peg behavior as an explicit operational outcome by directly linking price deviations to cash shortfalls within specified time windows. The coin issuer’s control mechanisms comprise two key instruments: the reallocation rate between immediately available cash and short-duration government bills, and the spread applied to mint or burn requests.

Methodologically, the control architecture combines stochastic model predictive control with a moment-closure forecast for Hawkes intensities and first-order conditions from Pontryagin’s maximum principle. This yields interpretable shadow prices for cash, bills, and peg deviation, and in turn produces implementable feedback rules. A settlement-window formulation converts the continuous problem into a sampled-data problem that matches wire cut-offs and repo calendars. In the discretized problem formulation, the rebalancing decision takes a soft-thresholding form driven by window-averaged costates, which provides a clear and auditable switching logic for treasury desks. We also establish a monotone stress-response property: as expected redemption pressure increases, as average ticket sizes grow, or as windows lengthen, the optimal policy tilts predictably toward cash. Conversely, the proposed algorithm enables efficient reallocation into higher-yielding government bonds during calm market phases, if time windows for reallocation decisions are chosen to be appropriately small.

The numerical experiments show how these design choices translate into outcomes that matter for issuers. Relative to a maximum-yield benchmark that waits until the last moment to raise liquidity, and a maximum-liquidity benchmark that forgoes carry, the window-based controller preserves most of the bill yield in calm conditions while moving earlier and more decisively when redemption risk rises. Because the policy depends only on filtered intensities, outstanding supply, and window-averaged shadow values, it fits daily treasury workflows and supports supervisory review. More broadly, the framework connects balance-sheet choices to market observables in a way that is

transparent: peg deviations emerge only when cash on hand is insufficient within a window, and the controller's reallocation speed and fee choices directly manage that risk.

A critical risk management concern is the tail probability of a complete depeg. Since such an event is close to catastrophic for the issuer, its probability warrants careful measurement even when it is very small. In this article we simulated 100 runs, which provides only limited estimation precision of probabilities below the one percent level. Future analyses can tighten this by running much larger simulation batches on specialized hardware, by applying dedicated rare-event techniques, or by developing analytical tail approximations.

Several extensions, both in terms of theoretical modeling and empirical validation, would deepen applicability of the proposed approach. Richer flow models with state-dependent trade sizes and cross-asset excitation, online estimation for time-varying branching ratios, robust or risk-sensitive MPC variants, and historical backtests with issuer data would allow closer alignment with specific mandates and regulatory constraints. Taken together, the contributions here provide a settlement-aware, interpretable, and auditable control system that turns reserve management into a disciplined optimization problem and offers a practical blueprint for resilient peg maintenance.

Acknowledgement(s)

The authors would like to thank TUM Blockchain Club for insightful discussions that helped shape the content of this manuscript.

Disclosure Statement

The authors report there are no competing interests to declare.

References

- [1] U.S. Congress, *Guiding and establishing national innovation for u.s. stablecoins act of 2025 (genius act)*, Public Law 119-XXX, enacted July 18, 2025 (2025). Available at <https://www.congress.gov/bill/119th-congress/senate-bill/394>.
- [2] E.A. Meyer, I.M. Welpe, and P. Sandner, *Decentralized Finance – A Systematic Literature Review and Research Directions*, in *Proceedings of the 30th European Conference on Information Systems (ECIS 2022)*, Timișoara, Romania. 2022, Available at <https://ssrn.com/abstract=4016497>.
- [3] B. Öz, B. Kraner, N. Vallarano, B.S. Kruger, F. Matthes, and C.J. Tessone, *Time Moves Faster When There is Nothing You Anticipate: The Role of Time in MEV Rewards*, in *Proceedings of the 2023 Workshop on Decentralized Finance and Security (DeFi '23)*, Copenhagen, Denmark. ACM, 2023.
- [4] D. Cumming, W. Drobetz, P.P. Momtaz, and N. Schermann, *Financing decentralized digital platform growth: The role of crypto funds in blockchain-based startups*, *Journal of Business Venturing* 40 (2025), p. 106450.
- [5] P.P. Momtaz, *The pricing and performance of cryptocurrency*, *The European Journal of Finance* 27 (2021), pp. 367–380.
- [6] L.T. Hoang and D.G. Baur, *How stable are stablecoins?*, *European Journal of Finance*

30 (2021), pp. 1984–2000, Available at <https://doi.org/10.1080/1351847x.2021.1949369>.

[7] K. Grobys, J. Juntila, J.W. Kolari, and N. Sapkota, *On the stability of stablecoins*, Journal of Empirical Finance 64 (2021), pp. 207–223, Available at <https://doi.org/10.1016/j.jempfin.2021.09.002>.

[8] K. Jarno and H. Kołodziejczyk, *Does the Design of Stablecoins Impact Their Volatility?*, Journal of risk and financial management 14 (2021), p. 42, Available at <https://doi.org/10.3390/jrfm14020042>.

[9] D.G. Baur and L.T. Hoang, *A crypto safe haven against Bitcoin*, Finance research letters 38 (2020), p. 101431, Available at <https://doi.org/10.1016/j.frl.2020.101431>.

[10] G.J. Wang, X.Y. Ma, and H.Y. Wu, *Are stablecoins truly diversifiers, hedges, or safe havens against traditional cryptocurrencies as their name suggests?*, Research in International Business and Finance 54 (2020), p. 101225, Available at <https://doi.org/10.1016/j.ribaf.2020.101225>.

[11] I.G.A. Pernice, *On stablecoin price processes and arbitrage*, SSRN Electronic Journal (2021), Available at https://papers.ssrn.com/sol3/papers.cfm?abstract_id=3793114.

[12] L. Ante, I. Fiedler, and E. Strehle, *The impact of transparent money flows: Effects of stablecoin transfers on the returns and trading volume of bitcoin*, Technological Forecasting and Social Change 170 (2021), p. 120851, Available at <https://doi.org/10.1016/j.techfore.2021.120851>.

[13] K. Grobys and T.L.D. Huynh, *When Tether says “JUMP!” Bitcoin asks “How low?”*, Finance research letters 47 (2021), p. 102644, Available at <https://doi.org/10.1016/j.frl.2021.102644>.

[14] C. Jeger, B. Rodrigues, E. Scheid, and B. Stiller, *Analysis of Stablecoins during the Global COVID-19 Pandemic*, in *Proceedings of the 2020 International Conference on Blockchain Computing and Applications (BCCA)*, Antalya, Turkey. 2020, pp. 30–37.

[15] J.M. Griffin and A. Shams, *Is bitcoin really un-tethered?*, SSRN Electronic Journal (2018), Available at <https://doi.org/10.2139/ssrn.3195066>.

[16] W.C. Wei, *The impact of Tether grants on Bitcoin*, Economics Letters 171 (2018), pp. 19–22, Available at <https://doi.org/10.1016/j.econlet.2018.07.001>.

[17] L. Kristoufek, *Tethered, or untethered? on the interplay between stablecoins and major cryptoassets*, Finance Research Letters 43 (2021), p. 101991, Available at <https://doi.org/10.1016/j.frl.2021.101991>.

[18] T.V.H. Nguyen, T.V.H. Nguyen, T.C. Nguyen, T.T.A. Pham, and Q.M.P. Nguyen, *Stablecoins versus traditional cryptocurrencies in response to interbank rates*, Finance Research Letters 47 (2022), p. 102744, Available at <https://doi.org/10.1016/j.frl.2022.102744>.

[19] M.M. Bojaj, M. Muhadinovic, A. Bracanovic, A. Mihailovic, M. Radulovic, I. Jolicic, I. Milosevic, and V. Milacic, *Forecasting macroeconomic effects of stablecoin adoption: A Bayesian approach*, Economic Modelling 109 (2022), p. 105792, Available at <https://doi.org/10.1016/j.econmod.2022.105792>.

[20] B.N. Thanh, T.N.V. Hong, H. Pham, T.N. Cong, and T.P.T. Anh, *Are the stabilities of stablecoins connected?*, Journal of Industrial and Business Economics 50 (2022), pp. 515–525, Available at <https://doi.org/10.1007/s40812-022-00207-3>.

[21] A. Jalan, R. Matkovskyy, and L. Yarovaya, *“Shiny” crypto assets: A systemic look at gold-backed cryptocurrencies during the COVID-19 pandemic*, International Review of Financial Analysis 78 (2021), p. 101958, Available at <https://doi.org/10.1016/j.irfa.2021.101958>.

[22] C. Aloui, H.B. Hamida, and L. Yarovaya, *Are Islamic gold-backed cryptocurrencies different?*, Finance research letters 39 (2020), p. 101615, Available at <https://doi.org/10.1016/j.frl.2020.101615>.

[23] I. Yousaf and L. Yarovaya, *Spillovers between the Islamic gold-backed cryptocurrencies and equity markets during the COVID-19: A sectorial analysis*, Pacific-Basin Finance Journal

71 (2021), p. 101705, Available at <https://doi.org/10.1016/j.pacfin.2021.101705>.

[24] M. Kjaer, M. Di Angelo, and G. Salzer, *Empirical Evaluation of MakerDAO's Resilience*, in *2021 3rd Conference on Blockchain Research & Applications for Innovative Networks and Services (BRAINS)*. 2021, pp. 193–200, Available at <https://doi.org/10.1109/brains52497.2021.9569811>.

[25] H. Uhlig, *A luna-tic stablecoin crash*, SSRN Electronic Journal (2022), Available at <https://doi.org/10.2139/ssrn.4165328>.

[26] A. Briola, D. Vidal-Tomás, Y. Wang, and T. Aste, *Anatomy of a stablecoin's failure: The terra-luna case*, Finance Research Letters 51 (2022), p. 103358, Available at <https://doi.org/10.1016/j.frl.2022.103358>.

[27] W. Zhao, H. Li, and Y. Yuan, *Understand Volatility of Algorithmic Stablecoin: Modeling, Verification and Empirical Analysis*, in *Financial Cryptography and Data Security*. Springer, 2021.